PROCEEDINGS OF SPIE

SPIEDigitalLibrary.org/conference-proceedings-of-spie

Small satellites with MEMS x-ray telescopes for x-ray astronomy and solar system exploration

Yuichiro Ezoe, Yoshizumi Miyoshi, Satoshi Kasahara, Tomoki Kimura, Kumi Ishikawa, et al.

Yuichiro Ezoe, Yoshizumi Miyoshi, Satoshi Kasahara, Tomoki Kimura, Kumi Ishikawa, Masaki Fujimoto, Kazuhisa Mitsuda, Hironori Sahara, Naoki Isobe, Hiroshi Nakajima, Takaya Ohashi, Haruki Nagata, Ryu Funase, Munetaka Ueno, Graziella Branduardi-Raymont, "Small satellites with MEMS x-ray telescopes for x-ray astronomy and solar system exploration," Proc. SPIE 10699, Space Telescopes and Instrumentation 2018: Ultraviolet to Gamma Ray, 106990V (6 July 2018); doi: 10.1117/12.2311422

SPIE.

Event: SPIE Astronomical Telescopes + Instrumentation, 2018, Austin, Texas, United States

Small satellites with MEMS X-ray telescopes for X-ray astronomy and solar system exploration

Yuichiro Ezoe[a], Yoshizumi Miyoshi[b], Satoshi Kasahara[c], Tomoki Kimura[d], Kumi Ishikawa[e], Masaki Fujimoto[e], Kazuhisa Mitsuda[e], Hironori Sahara[a], Naoki Isobe[e], Hiroshi Nakajima[f], Takaya Ohashi[a], Harunori Nagata[g], Ryu Funase[c], Munetaka Ueno[h], and Graziella Branduardi-Raymont[i]

[a]Tokyo Metropolitan University, 1-1 Minami-Osawa, Hachioji, Tokyo 192-0397, Japan;
[b]Nagoya University, Furo-cho, Chikusa-ku, Nagoya 464-8601, Japan;
[c]University of Tokyo, 7-3-1 Hongo, Bunkyo-ku, Tokyo 113-8654, Japan;
[d]Tohoku University, 6-6 Aoba, Aramakiaza, Sendai, Miyagi 980-8579, Japan;
[e]Institute of Space and Astronautical Science (ISAS), Japan Aerospace and eXpoloration Agency (JAXA), 3-1-1 Yoshinodai, Sagamihara, Kanagawa 229-8510, Japan;
[f]Kanto Gakuin University, 1-50-1 Rokuura higashi, Kanazawa-ku, Yokohama 236-8501, Japan;
[g]Hokkaido University, Kita 13 Nishi 8, Kita-ku, Sapporo 060-8628, Japan;
[h]Kobe University, 7-1-48 Minatojima-minamimachi, Chuo-ku, Kobe, Hyogo, 650-0047, Japan;
[i]Mullard Space Science Laboratory, University College London, Holmbury St Mary, Dorking, Surrey RH5 6NT, UK;

ABSTRACT

Toward a new era of X-ray astronomy, next generation X-ray optics are indispensable. To meet a demand for telescopes lighter than the foil optics but with a better angular resolution less than 1 arcmin, we are developing micropore X-ray optics based on micromaching technologies. Using sidewalls of micropores through a thin silicon wafer, this type can be the lightest X-ray telescope ever achieved. Two new Japanese missions ORBIS and GEO-X will carry this optics. ORBIS is a small X-ray astronomy mission to monitor supermassive blackholes, while GEO-X is a small exploration mission of the Earth's magnetosphere. Both missions need a ultra light-weight (<1 kg) telescope with moderately good angular resolution (<10 arcmin) at an extremely short focal length (<30 cm). We plan to demonstrate this optics in these two missions around 2020, aiming at future other astronomy and exploration missions.

Keywords: Micropore X-ray optics, Small satellites, ORBIS, GEO-X

1. INTRODUCTION

X-ray telescopes are essential for future X-ray astronomy. Toward a new era of X-ray astronomy, next generation X-ray optics are needed. Three different methods have been established in the past X-ray missions; direct polishing of glass, replication of thin shells from an accurately shaped mandrel, and thin foils bent to a conical approximation of a Wolter type-I geometry. As shown in figure 1, there is a well known trade-off relation between the angular resolution and the mass normalized by the effective area in these three methods.[1] In order to break this relation, new mirror fabrication methods are demanded.

There is an obvious need for telescopes as light as the foil optics but with <10 arcsecond angular resolution, which is ×10 better than the foil optics. Silicon pore optics, precision polishing of single-crystal silicon, slumping of glass sheets or adjustable optics with piezo stress are being developed for this purpose (e.g.,[2–4]). Such technologies are especially important for large X-ray observatories such as Athena and Lynx.

Further author information: (Send correspondence to Y.E.)
Y.E.: E-mail: ezoe@tmu.ac.jp

Space Telescopes and Instrumentation 2018: Ultraviolet to Gamma Ray, edited by Jan-Willem A. den Herder, Shouleh Nikzad, Kazuhiro Nakazawa, Proc. of SPIE Vol. 10699, 106990V · © 2018 SPIE
CCC code: 0277-786X/18/$18 · doi: 10.1117/12.2311422

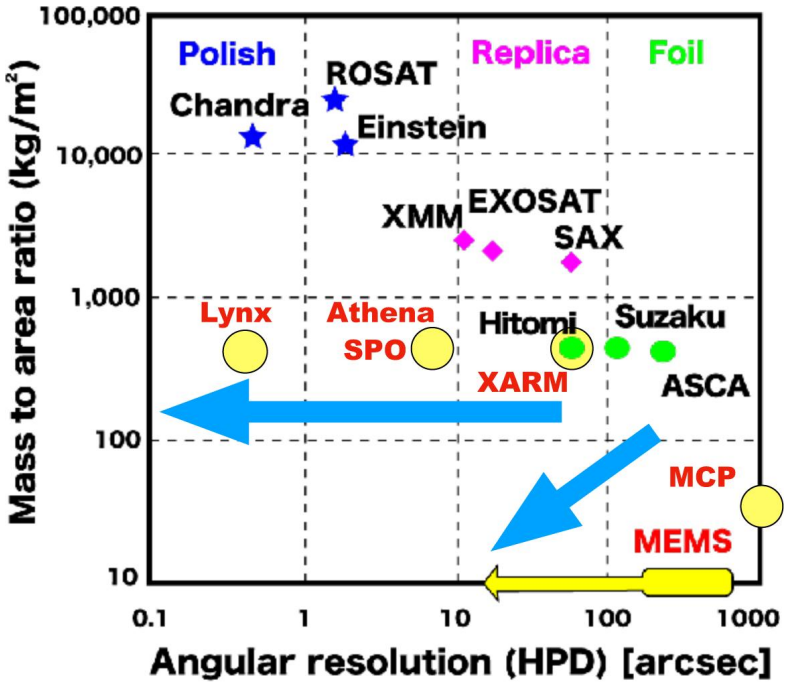

Figure 1. Performances of past and future X-ray telescopes. A horizontal axis is the angular resolution in half power diameter (HPD), while a vertical axis is a telescope mass normalized by an effective area at 1 keV. Stars, diamonds, and green circles represent X-ray telescopes onboard past space missions. Yellow circles are required performances in future missions or expected performances of micropore X-ray optics. Blue arrows indicate the two major demands in future missions. A goal of our MEMS X-ray optics is shown in an yellow arrow. This figure is revised from Bavdaz et al. (2004) and Ezoe et al. (2010).[1,10]

There is another demand for different telescopes that are lighter than the foil optics but have a comparable or better angular resolution of <1 arcmin. The next generation all sky monitor to cover a large fraction of the sky with focusing X-ray telescopes, small/medium class astronomy satellites, or solar system exploration missions can be listed as possible applications.

For these purposes, micropore X-ray optics are good candidates. Sidewalls of micropores through a thin substrate are utilized for X-ray mirrors. If we shrink the size of the mirrors in the telescope by a factor of C, the mirror weight decreases by C^3. To keep the same effective area, we have to increase the mirror number by C^2. Consequently, the telescope weight will decrease by C. Therefore, the smaller the micropores become, the lighter the telescope is.[5]

Three types of micropore optics have been proposed and are being developed. The first type is microchannel plate optics (MCP) made of glass fibers.[6–8] Sidewalls of square pores are utilzed for X-ray mirrors. A spherically bent glass plate with numerous micropores work as Lobster eye optics. By stacking two plates, Wolter type-I optics are also fabricated for the ESA's BepiColombo mission. The second type is the silicon pore optics called SPO.[1,2,7] A thin silicon wafer diced into rectangles is wedged and stacked on to another wafer so that the surface of the wafer is utilized for X-ray mirrors. This type is employed in the ESA's large X-ray observatory Athena.

As a third type, we have invented and are developing what we call MEMS X-ray optics.[5,9–14] MEMS stands for Micro Electro Mechanical Systems. We apply micromachining technologies for the micropore X-ray optics. To date, we have demonstrated X-ray reflection and imaging with various MEMS techniques. In this paper, we introduce two new Japanese small mission plans ORBIS and GEO-X that will carry the MEMS X-ray optics. We then show concept and recent development of the MEMS X-ray optics.

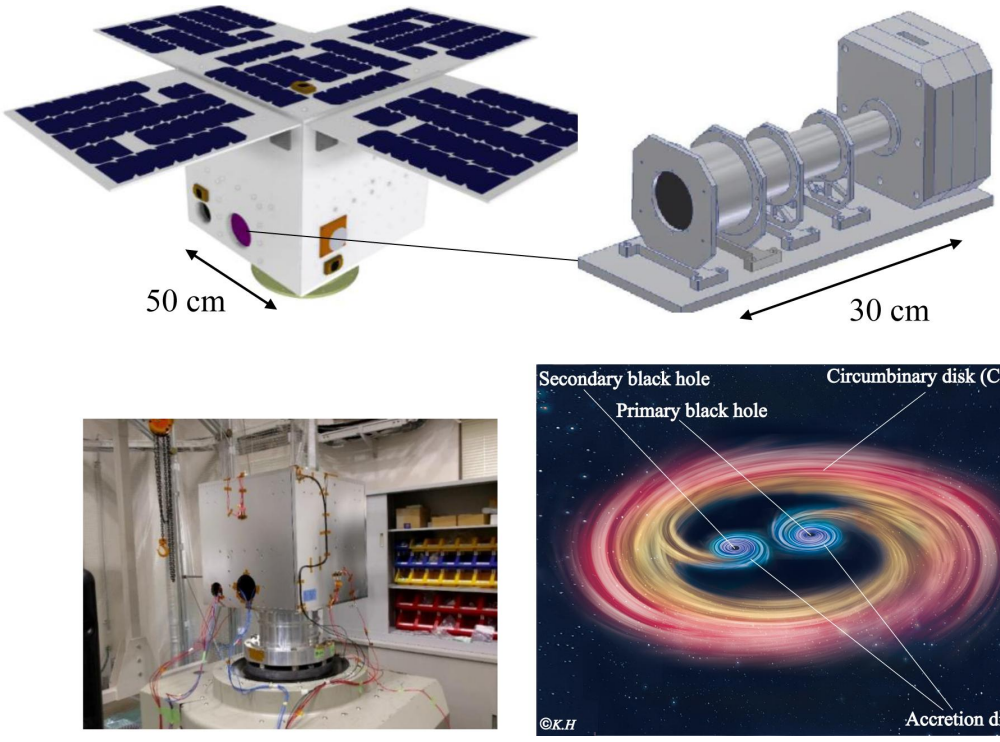

Figure 2. Overview of the ORBIS mission: (top) 3D cad drawings of the spacecraft and the payload, (bottom left) a photo of a structure and thermal model[15] and (bottom right) artistic impression of a BBH.[18]

2. SMALL MISSIONS

2.1 ORBIS

ORBIS (ORbiting Binary blackhole Investigation Satellite) is an University-built astronomy satellite led by Tokyo Metropolitan University in collaboration with ISAS/JAXA, Kanto Gakuin University, Kansei Gakuin University, Osaka University, and Meisei University.[15] Its science objective is to search for a signature of a binary black hole (BBH) by observing a specific active galactic nucleus (AGN) continuously for a long time (∼1 yr).

In spite of detections of gravitational waves from intermediate mass binary black holes, it is still unclear how a binary black hole evolves. In evolution of supermassive black holes in galactic nuclei, BBH(s) may form and influence their host galaxies. In the final stage of a BBH, the gravitational radiation becomes efficient to remove the angular momentum of the BBH. To reach this stage, the angular momentum must be lost while its loss by dynamical friction is expected to slow down due to depletion of stars on orbits intersecting the BBH.[16] As a possible scenario, a mass transfer from a circumbinary disk to each BH is suggested to add the angular momentum loss.[17] Furthermore, by combining the theoretical and observational studies, about 10 % of nearby AGNs with $10^{6.5-7}$ $M_{\odot}$ are estimated to be BBHs.[18] If so, there is a good chance to detect a binary signature. In fact, the optical observation of the blazer OJ287 over 100 years has revealed periodic bursts every ∼12 years and it is believed to be a BBH.[19]

The ORBIS mission is a special satellite dedicated to this science theme. It will observe only one or two specific AGNs in order to find out a binary motion. Such a observation focused on a limited target is unrealistic in large X-ray astronomy satellites. Even with all sky X-ray monitors, a nearly continuous observation of one target is not easy, because all sky X-ray monitors usually scan a part of the sky by narrowing the field of view with slits.[20] Therefore, the ORBIS can be a unique satellite complementary to large X-ray observatories and existing all sky monitors.

Figure 2 overviews the ORBIS satellite and its science payload. Specifications are summarized in table 1. It is 50 cm on a side with a mass of 50 kg including the science payload. Science requirements are shown in

Table 1. Specifications of the ORBIS satellite

	Unit	Values
Size	[mm]	500×500×500
Mass	[kg]	50
Power	[W]	144 (max)
Transmitter	[kbps]	100 (max) @ S-band
Receiver	[kbps]	1 (max) @ S-band
Altitude		550 km, Low Earth orbit

Table 2. Requirements and specifications of the science payload in ORBIS.

	Unit	Values
Energy	[keV]	0.3–10 keV
Point source sensitivity (3σ)	[mCrab]	5 in 3 days exposure
MEMS Wolter type-I X-ray optics		
Diameter	[mm]	100
Focal length	[mm]	250
Angular resolution	[arcmin]	<10 (HPD)
Mirror weight	[g]	5
CCD detector		
Pixel size	[μm]	24×24
Format	[pix]	320×256
Area	[mm]	7.680×6.114
Energy resolution	[eV]	180 at 6 keV
Operating temperature	[°C]	−90

table 2. A point source sensitivity comparable to an existing large all sky X-ray monitor MAXI[20] is required. To achieve this sensitivity under the limited resources (size, weight, and power), focusing the incident X-rays at a low-background detector is essential. Therefore, a compact X-ray imaging spectrometer composed of the MEMS X-ray optics and the CCD detector will be onboard. The MEMS X-ray optic can be a ultra-light weight telescope enabling a good angular resolution even at the required short focal length (<30 cm). The X-ray CCD is a miniature of the Hitomi SXI.[21]

We have constructed a structure and thermal model of the satellite. Environmental tests for this satellite model are on-going. In parallel, a vibration test for the MEMS Wolter type-I optics has been conducted and no damage on the optic was observed. We have started an assembly of a part of the flight model of the satellite. The payload will be assembled in the satellite in 2019. An aimed launch year is around 2020. A piggy back launch by a JAXA's H-IIA rocket is considered. A candidate for the science observation is a Seyfert 1 galaxy NGC 4151, which is suggested as a BBH candidate from an optical spectroscopy[22] and bright in X-rays. Other candidates such as a blazer Mrk 421 are under investigation. The line of sight direction is constrained by observational date and solar angle. We will finalize the target when a launch date is fixed.

2.2 GEO-X

GEO-X (GEOspace X-ray imager) is a small exploration satellite under concept study by Tokyo Metropolitan University, Nagoya University, University of Tokyo, ISAS/JAXA, Hokkaido University, Kanto Gakuin University, Kobe University, and Tohoku University. Its aim is X-ray imaging of the Earth's magnetosphere using solar wind charge exchange emission from a location outside the magnetosphere. For this purpose, the satellite will be located at the vicinity of the Moon which is about 60 $R_{\rm Earth}$ from the Earth and will observe this emission from that distant place for the first time.

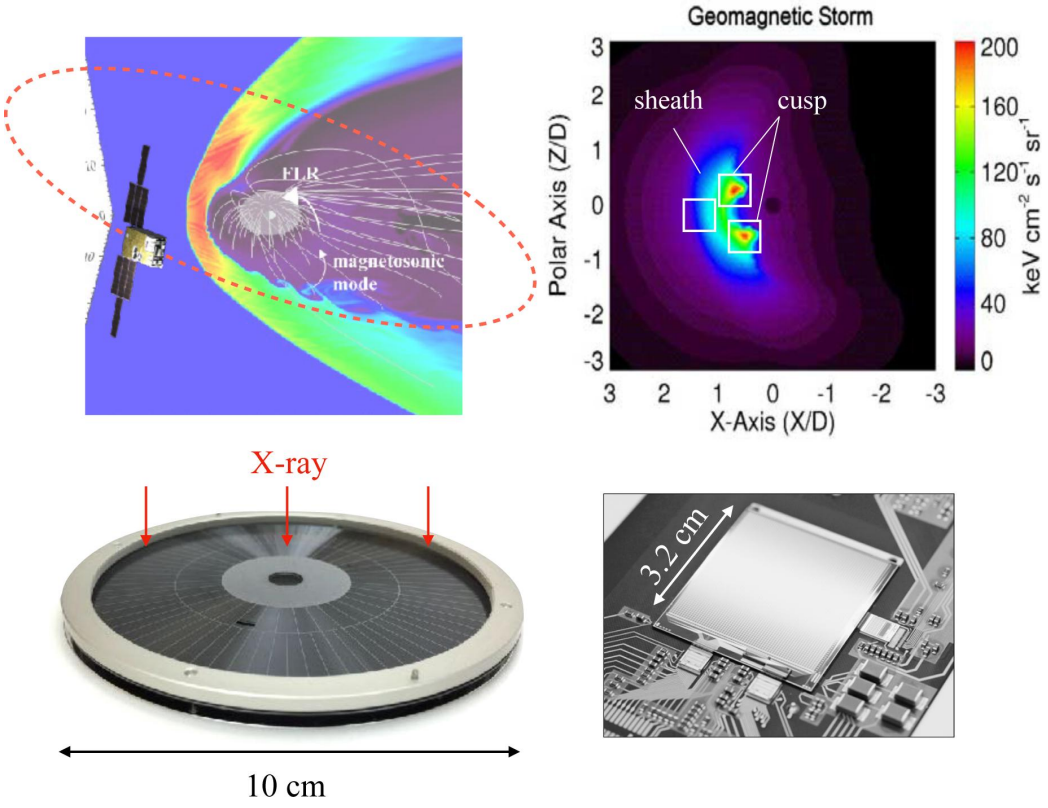

Figure 3. Overview of the GEO-X mission: (top left) a concept of the spacecraft orbiting around the Earth's magnetosphere,[29] (top right) a MHD-based model for the solar wind charge exchange emission as observed from 50 $R_{\rm Earth}$,[30] (bottom left) a MEMS Wolter type-I optic and (bottom right) a DepFET detector.[31] Solid squares in the MHD simulation indicate a FOV of the payload.

The solar wind charge exchange emission around the Earth was discovered with ROSAT during the all sky survey.[23] It occurs between solar wind ions and exospheric neutrals near the Earth. The solar wind ion such as O^{7+} strips an electron from the neutral atom or molecule such as H. The transferred electron to the ion decays into the ground state emitting photons as emission lines in the UV and X-ray wavelength range. Thanks to good energy resolution CCDs onboard Chandra, XMM-Newton and Suzaku, it is now established as a time-variable foreground emission for X-ray astronomy satellites orbiting around the Earth.[24–28]

Because these large X-ray observatories have relatively small FOVs (e.g., 20 arcmin×20 arcmin) and basically fly within the magnetosphere, fundamental questions such as how this emission is distributed and how this emission becomes bright are still unclear. Understanding of the solar wind charge exchange emission around the Earth is closely related to how the charge exchange emission occurs in other space environments such as supernova remnants and clusters of galaxies. Furthermore, from the viewpoint of planetary and magnetospheric science, this emission can be a new diagnostic tool to image the invisible Earth's magnetosphere.

Many model studies have been conducted on this X-ray emission using magnetohydrodynamics (MHD) simulations of the Earth's magnetosphere. The X-ray emission is predicted to be strong at the dayside sheath region where both solar wind density and exospheric density are high. Magnetosheath, cusps, and bowshock can be visualized via X-rays (e.g.,[30]). These dayside regions of the magnetosphere are especially of importance in the context of interactions between solar wind and the magnetosphere. To date, precise measurements of electromagnetic fields and plasmas have been done by in-situ observations. X-rays can be a new tool to take a global picture of the magnetosphere. Since the emission is expected to be associated with the magnetosphere, we basically need to escape from the magnetosphere.

Table 3. Specifications of the GEO-X satellite under concept study. Numbers are to be determined.

	Unit	Values
Size	[mm]	∼200×200×300
Mass	[kg]	∼30
Power	[W]	∼100 (max)
Transmitter	[kbps]	∼50 @ S-band
Receiver	[kbps]	∼1 @ S-band
Altitude		∼40-60 $R_{\rm Earth}$, High Earth orbit

Table 4. Requirements and specifications of the science payload in GEO-X.

	Unit	Values
Energy	[keV]	0.3–2 keV
Grasp	[cm^2 deg^2]	10 at 0.6 keV
MEMS Wolter type-I X-ray optics		
Diameter	[mm]	100
Focal length	[mm]	250
Angular resolution	[arcmin]	<10 (HPD)
Mirror weight	[g]	5
DepFET detector		
Pixel size	[μm]	300×300
Format	[pix]	64×64
Area	[mm]	19.2×19.2
Energy resolution	[eV]	80 at 1 keV
Operating temperature	[°C]	−60

GEO-X is a small satellite focusing on this special science theme. It will carry a wide FOV X-ray imaging spectrometer to map the emission with high sensitivity in 0.3–2 keV where the solar wind charge exchange emission is most strong as emission lines from ionized C, N, O, Fe, Mg, and S. The line of sight direction will be always toward the subsolar side of the Earth, i.e., near the dayside of the Earth. The satellite will be injected into high Earth orbit, outside the Earth's magnetosphere where the emission comes from. Similar to ORBIS, such observations have not been conducted.

Figure 3 shows a concept of the GEO-X satellite. Tables 3 and 4 summarize specifications of the satellite and the payload. The satellite will be a ∼12 U cubesat or a similar size. It will be injected into a near circular High Earth orbit with an altitude of 40-60 $R_{\rm Earrth}$, i.e., near the Moon and a small inclination angle. A propulsion system composed of N_2O and polyethylene can be attached to the satellite. The total weight of the satellite including the proplusion system will be ∼50 kg or less. A piggy back launch of the JAXA's HII-A or HIII rocket is considered. Necessary Δv depends on the rocket and its orbital insertion but it will be at most ∼400-500 m/s when the satellite is first injected into an elliptical orbit by the rocket with an apogee of ∼60,000 km.

To achieve a good sensitivity to this diffuse X-ray emission, a grasp or a multiple of an effective area and FOV is important. GEO-X will achieve a large grasp comparable to the Suzaku X-ray CCD and telescope system in this small satellite platform. It is in principle possible because of its short focal length and operation in the soft X-ray band, resulting in a huge FOV of $4^\circ \times 4^\circ$ at least. The required angular resolution is moderate because the X-ray emission is expected to be widely extended. The same Wolter type-I design as in ORBIS will be adopted, allowing us swift development. The aimed launch year is around 2022, near the next solar maximum.

We have estimated the number of events that GEO-X will detect using past solar wind data taken with the GOES and ACE satellites during 1998-2011. This duration covers one solar cycle. Here we assumed that signals are proportional to an incoming ion flux, while the background is a combination of soft X-ray sky background and non X-ray background. For simplicity, we focused on the O^{6+} K_α band (0.5–0.6 keV). From Robertson et al. (2006),[30] the X-ray flux at a certain solar wind O7+ flux level can be estimated. The soft X-ray background

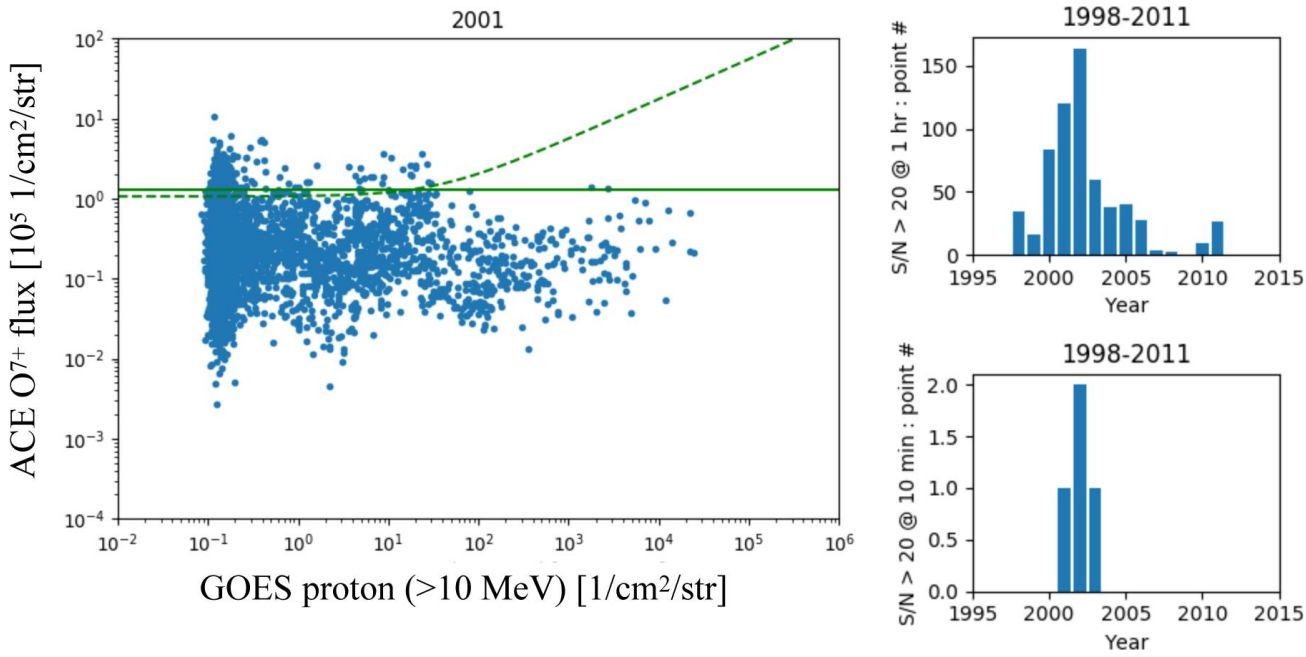

Figure 4. Example of GOES proton (>10 MeV) flux versus ACE O^{7+} flux in 2001, where each data point is 2 hr average. Solid and dashed lines indicate boundaries of the data points having signal to noise ratios (S/N) >20 when photon statistics or background fluctuation is considered, respectively. GEO-X instrumental parameters and an exposure time of 1 hr is assumed. On the right side, histograms of the number of points having S/N>20 in the 1 hr or 10 min exposure are plotted s a function of year from 1998 to 2011.

and the instrumental background including a radiation noise mainly due to high energy protons were calculated from the past X-ray observations[32] and our GEANT4 simulations.[33]

Figure 4 shows the results. We counted how many data points can meet the S/N ratio >20 based on the solar wind data and the past X-ray astronomy observations. The number of the data points can be converted to an estimated observational duration in which the high S/N ratio is expected. The estimated number of such data points peak around the solar maximum and decrease toward the solar minimum. At the solar maximum, about ∼150 data points exist, which indicate that we can obtain 300 data sets having S/N>20 at the 1 hr exposure time in a single year with GEO-X. Even at a 10 min exposure, good data points exist. On the other hand, at the solar minimum, the number of the data points are nearly zero. Therefore, the launch year is crucial. The most proper launch year would be early 2020's in which the solar activity will rise.

For the same purpose, i.e., X-ray imaging of the Earth's magnetosphere, the SMILE and CuPID missions are planned in ESA-China and USA, respectively.[34,35] The SMILE mission is a medium-class satellite observing the solar wind charge exchange emission from an elliptical orbit with an apogee of $\sim 20\ R_{\rm Earth}$. The orbit has a high inclination angle to observe UV aurora at the same time. Wide FOV Lobster MCP optics and a large format CCD will be onboard. The CuPID mission is a 6U cubesat at low Earth orbit and will carry Lobster MCP optics and a MCP detector. In contrast, GEO-X will observe this emission from the most distant place with a relatively small inclination angle, allowing unique sideview imaging of the Earth's magnetosphere. Also the DepFET detector is not significantly affected for optical light contamination, enabling observations of cusps near the dayside of the Earth. These features will make GEO-X unique and complimentary to the other missions.

3. MEMS X-RAY OPTICS

3.1 Concept

We utilize micromachining techniques for fabrication of the micropore X-ray optics. We have tested various techniques including anisotropic wet etching, deep reactive ion etching (DRIE), X-ray LIGA (Lithographie, Galvanik

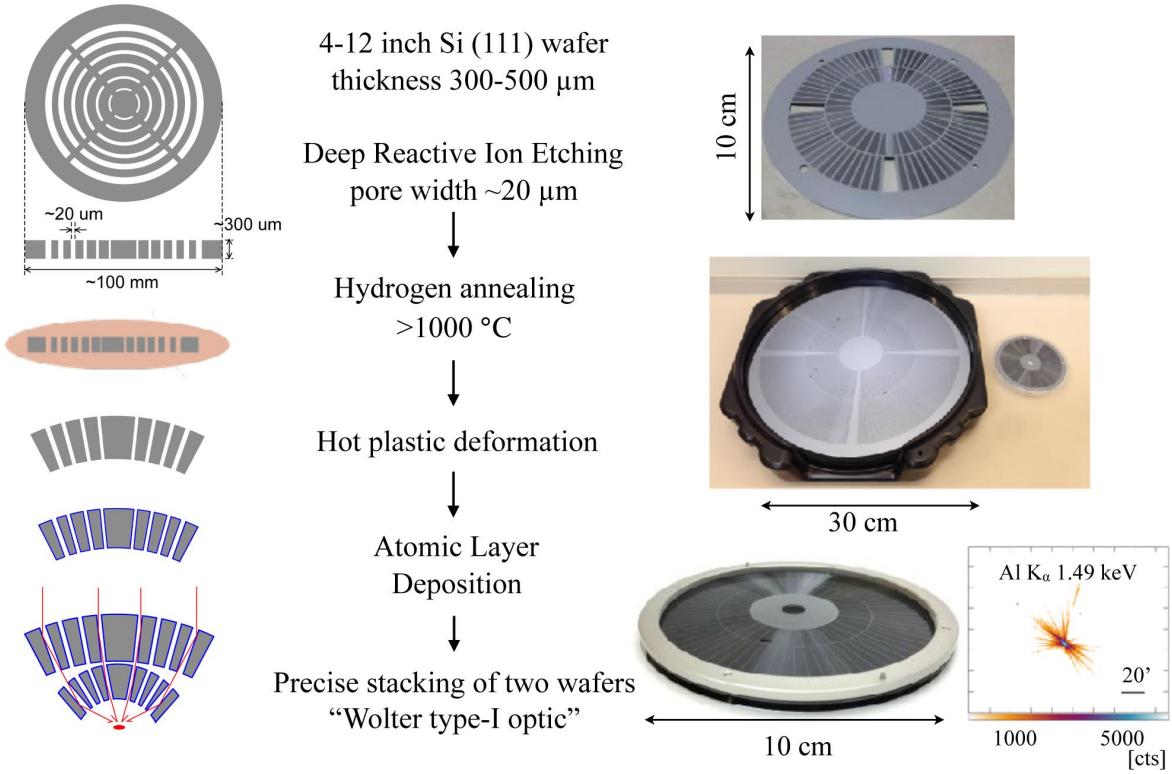

Figure 5. Process flow of the MEMS X-ray optics. From top to bottom, photos show a single-stage 4-inch Si optic, a 12-inch Si optic, and a 4-inch Wolter type-I optic.

und Abformung) and focused ion beam, and succeeded to verify X-ray reflection on sidewalls of micropores.[9, 10, 14] Now we focus on the DRIE-fabricated optics. The process flow is shown in figure 5.

Sidewalls of curvilinear micropores made by DRIE are smoothed by hydrogen annealing at >1000 C°. The wafer is deformed to a spherical shape by hot plastic deformation. Sidewalls can be coated with a high-Z material by Atomic Layer Deposition (ALD). Two wafers deformed to different curvature radii are precisely stacked to form a Wolter type-I optic. Because of the tiny pores and thin wafers, the MEMS X-ray optics can be the lightest X-ray telescope ever achieved. It is also low-cost because we basically fabricate the optics by ourselves.

A conical approximation of the Wolter type-I is almost negligible $\sim$ 2 arcsec even at a short focal length of 25 cm when the wafer thickness is 300 μm and the reflection angle is 1 deg. A theoretical limit on the angular resolution is an X-ray diffraction within each micropore which is $\sim$13 arcsec at 1 keV when the micropore width is 20 μm. Therefore, an ultra light-weight telescope with an angular resolution better than 1 arcmin would be possible. We have verified X-ray reflection and imaging with this method as shown in figure 5.

3.2 Design

Table 5 summarizes the baseline design of the MEMS Wolter type-I optic for ORBIS and GEO-X. The optic will be made from 4-inch Si wafers. An open area ratio will be $\sim$20 %. Sidewalls will be coated by Pt. A thin Al_2O_3 layer will be between Si and Pt for good adhesion. Figure 6 display raytracing simulations based on these parameters. A photon number for each simulation is 50,000. A detector size of 20 mm$\times$20 mm is used considering the GEO-X configuration. The focused image changes depending on the incident angle due to vignetting and stray light. We estimate an effective area and a grasp by integrating a r1.5 mm area around the focus. Figure 7 shows the obtained results.

In ORBIS, an on-axis effective area is crucial because the target is a point source and the line of sight direction will be always toward the target. A moderate effective area of $\sim$3 cm^2 is expected at 1 keV. Here the

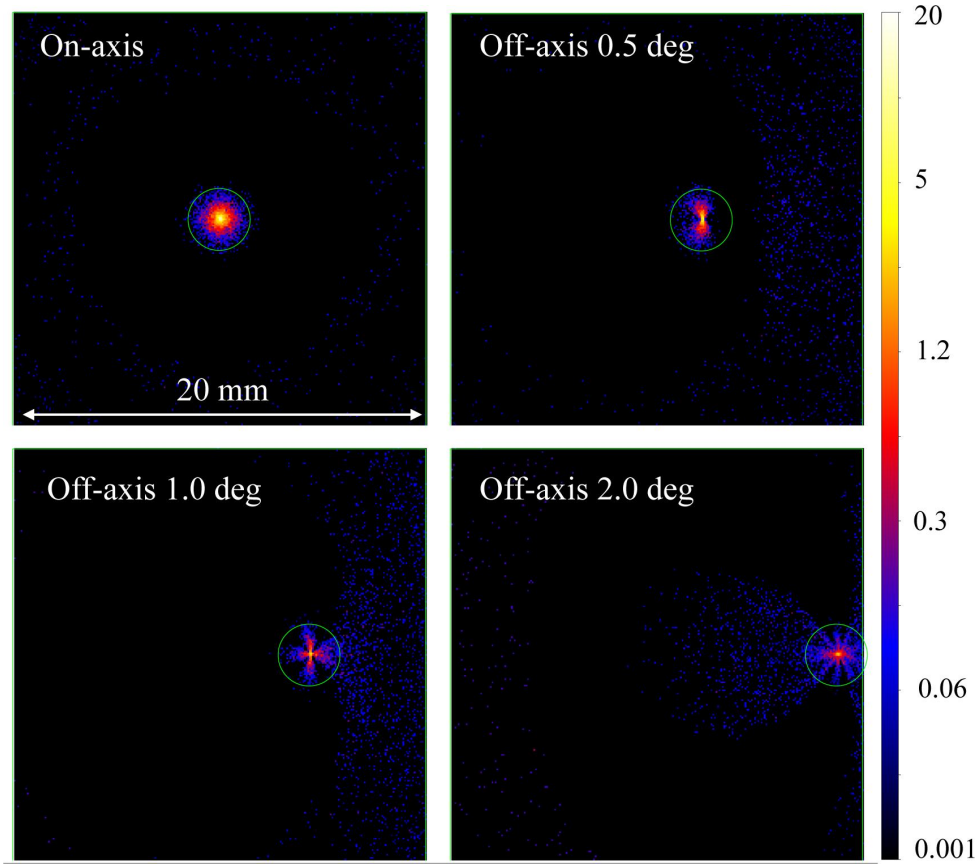

Figure 6. Raytracing results for the MEMS Wolter type-I optic assuming optics parameters in table 5 at 0.6 keV. Different incident angles are used. A color scale is in arbitrary unit. A solid circle corresponds to r1.5 mm.

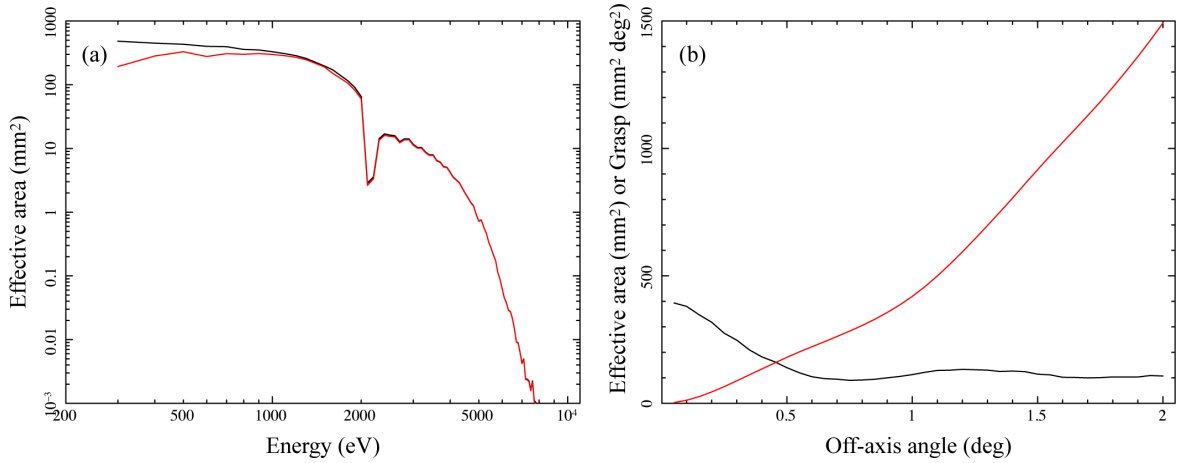

Figure 7. (a) Effective area of the MEMS Wolter type-I optic estimated from the raytracing simulations. Black and red curves represent an effective area without and with a detector quantum efficiency and an optical blocking filter. (b) Grasp of the MEMS Wolter type-I optic as a function of off-axis angle. Black and red curves are an effective area and a grasp. The detector and optical blocking filter efficiency is not included.

Table 5. Baseline design of the MEMS Wolter type-I optics for ORBIS and GEO-X.

	Unit	Values
Wafer properties		
Diameter	[mm]	100
Thickness	[μm]	300
Curvature radius	[mm]	1000 (1st), 333 (2nd)
Micropore properties		
Micropore width	[μm]	20
Space between micropores	[μm]	20
Innermost radius	[mm]	15
Outermost radius	[mm]	45
Sidewall coating		Pt+Al_2O_3
Required performance		
Angular resolution	[arcmin]	10
Effective area	[cm^2]	3 at 1 keV
Grasp	[cm^2 deg^2]	10 at 0.6 keV

detector quantum efficiency and the optical blocking filter of the Hitomi SXI are assumed. This value is a factor of ∼100 smaller than that of Suzaku XIS. However, the sensitivity to the point source is proportional to a square root of the effective area and the exposure time when the photon statistics or the background noise dominates. Therefore, because of the observation strategy that only a specific target is observed, the required sensitivity of 5 mCrab in 3 days exposure time can be achieved as far as the background level is similar to the Suzaku XIS. We expect to achieve such a low background in ORBIS because the orbit and the detector shield will be similar to those in Suzaku.

In GEO-X, a grasp is more important. Because of the large field of view, a grasp will be comparable to or even better than that of Suzaku XIS. The calculated value is 1500 mm^2 deg^2 or 15 cm^2 deg^2 at 0.6 keV. After considering the detector and optical blocking filter efficiency, which will be similar to ORBIS (∼70% at 0.6 keV and >90 % above 1 keV), the required grasp of >10 cm^2 deg^2 will be satisfied. Thus, these simulations indicate that the compact and light-weight MEMS Wolter type-I optic can meet the required sensitivity in ORBIS and GEO-X under the very limited resources of these small missions.

3.3 Recent development

Below we briefly introduce our recent development of the MEMS X-ray optics toward ORBIS and GEO-X. As described above, we have fabricated and demonstrated the Wolter type-I optic. We are now improving the angular resolution and the effective area so that the required parameters are satisfied.

3.4 Angular resolution

From a series of evaluations of mirror qualities and arrangement errors in a step by step manner at individual processes, we now consider that one of the major factors for the angular resolution is mirror quality itself. Figure 8 (a) shows our recent X-ray test of a single mirror. It has a relatively sharp peak with a half energy width of ∼5 arcmin on average within the optic. A typical FWHM is ∼3 arcmin. The required value by single reflection is 5 arcmin in both ORBIS and GEO-X. Therefore, this main component seems to meet the requirement.

There are two components in the single mirror response that should be eliminated or reduced. One is a broad component represented by a Lorentzian model. A half energy width of this component is typically ∼15 arcmin. As a result, the half energy width of the peak becomes worse by a factor of ∼1.5. The angular distribution of the Lorentzian component is similar to expected X-ray scattering from the mirror surface power spectrum density (PSD). Therefore, we are now trying to suppress the surface roughness by changing DRIE and annealing processes. Because the X-ray scattering intensity is proportional to the PSD and the rms roughness is an integral of the PSD in the frequency domain, we aim at a factor of ∼3 reduction of the rms roughness which leads to a factor of ∼9 reduction of the scattering intensity if this is the case.

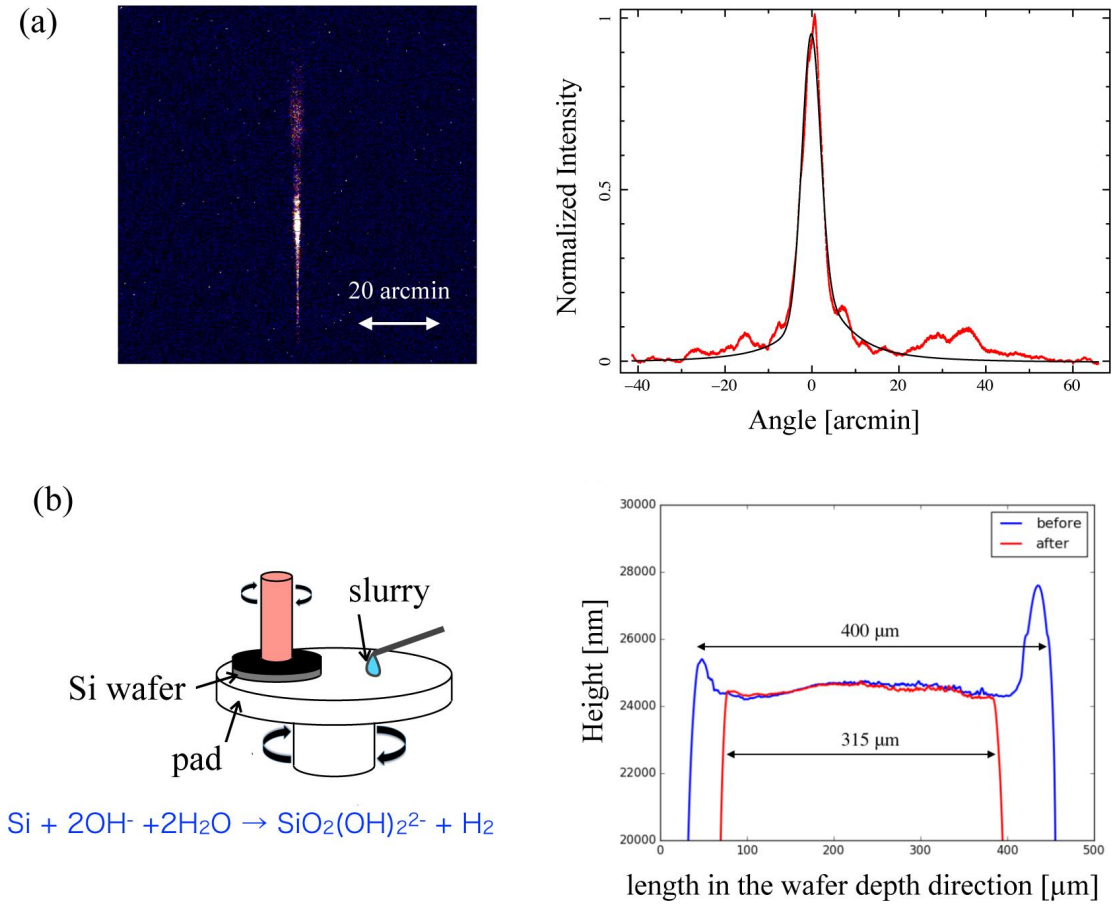

Figure 8. (a) X-ray response of a single mirror after DRIE and annealing at Al K_α 1.49 keV and its projected profile fitted with Gaussian and Lorentzian models. (b) Concept of chemical mechanical polishing and an example of sidewall profiles of a sample DRIE-fabricated optic before and after polishing.

The other unwanted component is an additional peak located at large reflection angles. It is most likely due to edge structures in the sidewalls generated after DRIE. We thus newly introduced chemical mechanical polishing of the wafer after DRIE from both sides. We filled micropores with photoresist in order not to break structures and removed the photoresist after polishing. As shown in figure 8 (b), we succeeded to remove the edge structures without destruction of the wafer. Thus, we now can expect a better angular response.

3.5 Effective area

In addition to the angular resolution, we also tried a new ALD process to increase the effective area.[36] We have tested Ir ALD in the early stage of our development.[37] Although the coating was successful in terms of X-ray reflectivity, the cost was higher. The Pt ALD process consists of two reactions. At first, we introduce a Pt precursor 2(MeCp)$PtMe_3$. Then, the precursor attached to the wafer surface is catalytically combusted by O_2. By cycling these two reactions, a pure Pt layer can be coated on the Si sidewalls. The reaction temperature and the growth rate are ∼270 °C and ∼0.4 Å/cycle, respectively. To strengthen adhesion, we inserted an Al_2O_3 layer bewteen Si and Pt.

Figure 9 shows an example of the MEMS X-ray optic after DRIE, annealing and ALD. A transmission electron microscope image of a sidewall indicates that the two layers are coated properly on the sidewall. At Al K_α 1.49 keV, an enhanced X-ray reflectivity was confirmed. However, the surface roughness estimated from the curves seemed to increase after coating from 1.6 to 2.2 nm rms. Therefore, we coated another wafer with a different

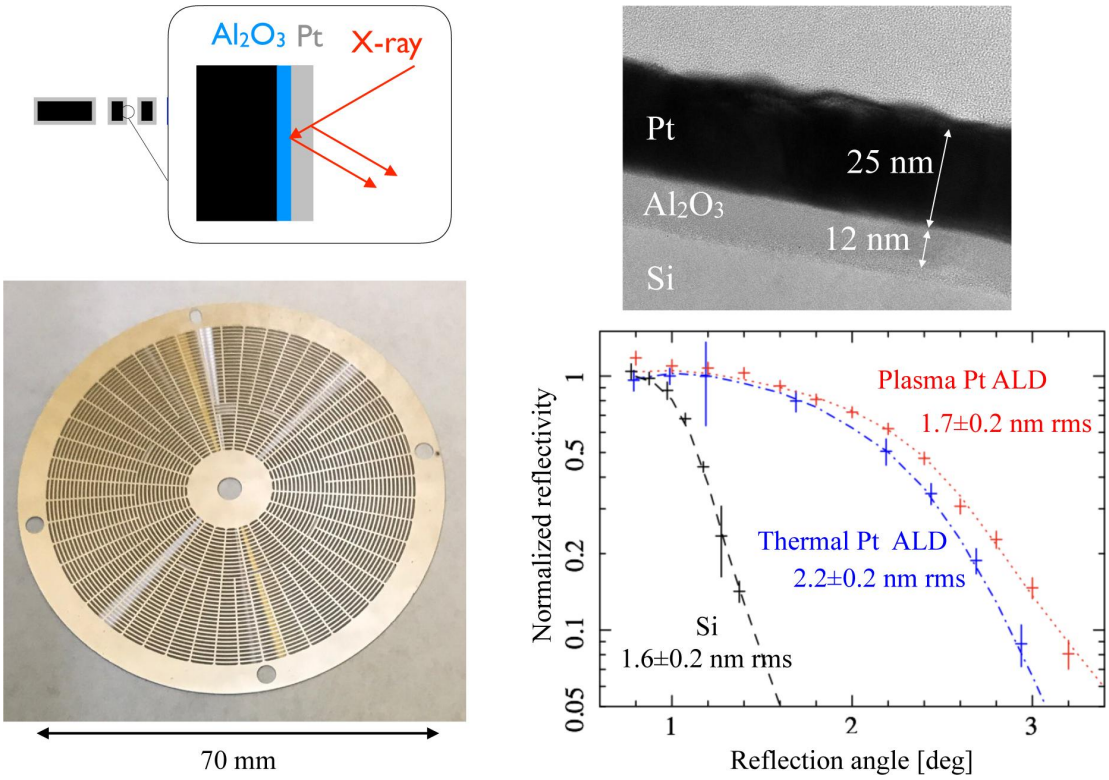

Figure 9. (Top and bottom left) Concept and photo of Pt-coated MEMS X-ray optics, (Top right) a transmission electron microscope image of a sidewall, and (Bottom right) X-ray reflectivity curves at Al K_α 1.49 keV of the sidewalls. The photo and electron microscope image are for the Plasma Pt ALD sample, while the reflectivity curves are for both the thermal and plasma Pt ALD samples.

ALD method. To activate chemical reactions, we introduced O plasma instead of O_2 gas. This process is called Plasma ALD and distinguished by the previous process, thermal ALD.

Consequently, the Plasma ALD coated sample showed a better reflectivity while the surface roughness before coating was the same as that before the thermal ALD. No significant change in the microroughness was observed. The required microroughness in ORBIS and GEO-X is below ∼1.5 nm rms. Therefore, these results support the view that the Pt coating by ALD is usable to enhance the effective area of the MEMS X-ray optics.

We plan to start fabricating the flight model Wolter type-I optics for ORBIS GEO-X soon. New technologies under testing to improve the angular resolution and the effective area are promising. In parallel, shock and thermal tests for a test optic will be conducted. We hope to finish all these development items within the schedule and launch the two optics in early 2020's.

4. SUMMARY

To summarize, future small missions such as ORBIS and GEO-X need new ultra light-weight telescopes with a moderate angular resolution at a short focal length and/or a wide field of view. Our MEMS X-ray optics is ideal for these purposes. We have demonstrated X-ray reflection and imaging with this method. Now we are improving the angular resolution and the effective area by introducing new cutting edge technologies. We hope to verify this new telescope in ORBIS and GEO-X and then other small or medium satellite missions as well as solar system explorations to Jupiter or Mars in late 2020's, Figure 10 shows simulated images using a ROSAT all sky survey 3/4 keV band image near the Galactic center. Our final goal is to achieve the comparable angular resolution to the ROSAT all sky survey.

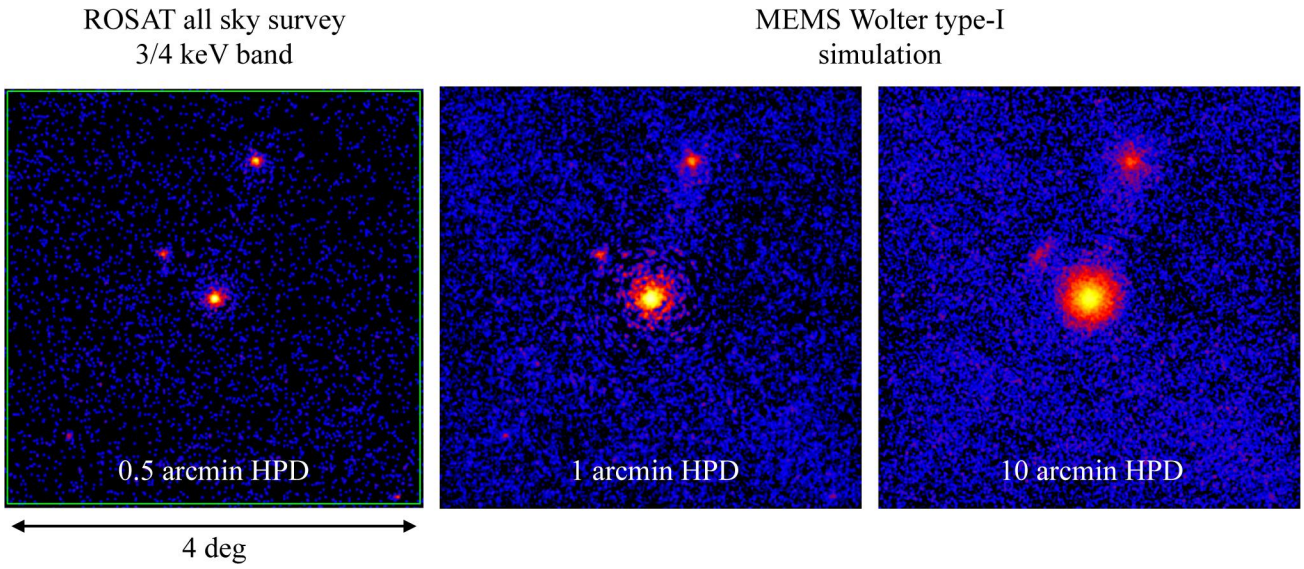

Figure 10. MEMS Wolter type-I simulations compared to an original ROSAT all sky survey 3/4 keV band image near the Galactic center (ra, dec) = (266.404996, 28.936172) in J2000.[38] The telescope parameters are as in table 5. An X-ray energy of 0.6 keV is assumed.

ACKNOWLEDGMENTS

This work was supported by MEXT KAKENHI grant number 20684006, 23684009, and 26287032, Toray science and technology grant, and MEXT promotion grant for aerospace science.

REFERENCES

[1] Bavdaz, M., Lumb, D. H., Peacock, A., Beijersbergen, M., and Kraft, S., "Development of x-ray optics for the XEUS Mission," in [*Society of Photo-Optical Instrumentation Engineers (SPIE) Conference Series*], Snigirev, A. A. and Mancini, D. C., eds., *Proc. SPIE* **5539**, 95–103 (2004).

[2] Bavdaz, M., Wille, E., Ayre, M., Ferreira, I., Shortt, B., Fransen, S., Collon, M., Vacanti, G., Barriere, N., Landgraf, B., Haneveld, J., van Baren, C., Zuknik, K.-H., Della Monica Ferreira, D., Massahi, S., Christensen, F., Krumrey, M., Burwitz, V., Pareschi, G., Spiga, D., Valsecchi, G., Vernani, D., Oliver, P., and Seidel, A., "The ATHENA telescope and optics status," in [*Society of Photo-Optical Instrumentation Engineers (SPIE) Conference Series*], *Proc. SPIE* **10399**, 103990B (2017).

[3] Zhang, W. W., Allgood, K. D., Biskach, M. P., Chan, K.-W., Hlinka, M., Kearney, J. D., Mazzarella, J. R., McClelland, R. S., Numata, A., Olsen, L. G., Riveros, R. E., Saha, T. T., and Solly, P. M., "Monocrystalline silicon and the meta-shell approach to building x-ray astronomical optics," in [*Society of Photo-Optical Instrumentation Engineers (SPIE) Conference Series*], *Proc. SPIE* **10399**, 103990S (2017).

[4] Cotroneo, V., Allured, R., DeRoo, C. T., Gurski, K. L., Marquez, V., Reid, P. B., and Schwartz, E. D., "Thermal forming of glass substrates for adjustable optics (Conference Presentation)," in [*Society of Photo-Optical Instrumentation Engineers (SPIE) Conference Series*], *Proc. SPIE* **10399**, 103990Y (2017).

[5] Ezoe, Y., Koshiishi, M., and Mitsuda, K., [*MEMS open the way to ultra-lightweight and low-cost x-ray optics*], SPIE Newsroom (2006). http://spie.org/x8595.xml.

[6] Wilkins, S. W., Stevenson, A. W., Nugent, K. A., Chapman, H., and Steenstrup, S., "On the concentration, focusing, and collimation of x-rays and neutrons using microchannel plates and configurations of holes," *Rev. Sci. Instrum.* **60**, 1026–1036 (1989).

[7] Bavdaz, M., Collon, M., Beijersbergen, M., Wallace, K., and Wille, E., "X-ray pore optics technologies and their application in space telescopes," *X-Ray Opt. Instrum.* **2010**, 295095 (2010).

[8] Fraser, G. W., Carpenter, J. D., Rothery, D. A., Pearson, J. F., Martindale, A., Huovelin, J., Treis, J., Anand, M., Anttila, M., Ashcroft, M., Benkoff, J., Bland, P., Bowyer, A., Bradley, A., Bridges, J., Brown, C., Bulloch, C., Bunce, E. J., Christensen, U., Evans, M., Fairbend, R., Feasey, M., Giannini, F., Hermann, S., Hesse, M., Hilchenbach, M., Jorden, T., Joy, K., Kaipiainen, M., Kitchingman, I., Lechner, P., Lutz, G., Malkki, A., Muinonen, K., Näränen, J., Portin, P., Prydderch, M., Juan, J. S., Sclater, E., Schyns, E., Stevenson, T. J., Strüder, L., Syrjasuo, M., Talboys, D., Thomas, P., Whitford, C., and Whitehead, S., "The mercury imaging X-ray spectrometer (MIXS) on bepicolombo," *Planet. Space. Sci.* **58**, 79–95 (2010).

[9] Ezoe, Y., Koshiishi, M., Mita, M., Mitsuda, K., Hoshino, A., Ishisaki, Y., Yang, Z., Takano, T., and Maeda, R., "Micropore x-ray optics using anisotropic wet etching of (110) silicon wafers," *Appl. Opt.* **45**, 8932–8938 (2006).

[10] Ezoe, Y., Mitsuishi, I., Takagi, U., Koshiishi, M., Mitsuda, K., Yamasaki, N., Ohashi, T., Kato, F., Sugiyama, S., Riveros, R., Yamaguchi, H., Fujihira, S., Kanamori, Y., Morishita, K., Nakajima, K., and Maeda, R., "Ultra light-weight and high-resolution x-ray mirrors using drie and x-ray liga techniques for space x-ray telescopes," *Microsys. Tech.* **16**, 1633–1641 (2010).

[11] Yamaguchi, H., Riveros, R., Mitsuishi, I., Takagi, U., Ezoe, Y., Yamasaki, N., Mitsuda, K., and Hashimoto, F., "Magnetic field assisted finishing for micro-pore x-ray focusing mirrors fabricated by deep reactive ion etching," *CIRP Annals-Manufacturing Technologies* **59**, 351–354 (2010).

[12] Riveros, R., Yamaguchi, H., Mitsuishi, I., Takagi, U., Ezoe, Y., Kato, F., Sugiyama, S., Yamasaki, N., and Mitsuda, K., "Development of an alternating magnetic field assisted finishing process for mems micro-pore x-ray optics," *Appl. Opt.* **49**, 3511–3521 (2010).

[13] Ezoe, Y., Moriyama, T., Ogawa, T., Kakiuchi, T., Mitsuishi, I., Mitsuda, K., Aoki, T., Morishita, K., and Nakajima, K., "Large aperture focusing of x-rays with micro pore optics using dry etching of silicon wafers," *Optics Letters* **37**, 779–781 (2012).

[14] Numazawa, M., Ezoe, Y., Ishikawa, K., Ogawa, T., Sato, M., Nakamura, K., Takeuchi, K., Terada, M., Ohashi, T., and Mitsuda, K., "First demonstration of x-ray mirrors using focused ion beam," *Japanese J. Appl. Phys.* **55**, 6S1 (2016).

[15] Matsushima, J., Sahara, H., Asano, S., Kaku, M., Kanda, T., Banno, M., Asano, H., Kobayashi, Y., Kimura, N., Yamashita, N., Ezoe, Y., Ishikawa, K., Nakamura, K., Numazawa, M., Takeuchi, K., Terada, M., Ishi, D., Noda, Y., Fujitani, M., Isobe, N., Nakajima, H., and Miyamura, N., "Development of Binary Black Hole Observation Satellite "ORBIS"," *Trans. of Japan Soc. for Astron. Space Sci.* (inpress).

[16] Merritt, D. and Milosavljevic′, M., "New orbit solutions for the precessing binary black hole model of oj 287," *Living Rev. Relativity* **8**, 8 (2005).

[17] Hayasaki, K., "A new mechanism for massive binary black-hole evolution," *Publ. Astron. Soc. Japan* **61**, 65–74 (2009).

[18] Hayasaki, K., Ueda, Y., and Isobe, N., "Mass function of binary massive black holes in active galactic nuclei," *Publ. Astron. Soc. Japan* **62**, 1351–1360 (2010).

[19] Valtonen, M. J., "New orbit solutions for the precessing binary black hole model of oj 287," *Astrophys. J.* **659**, 1074–1081 (2007).

[20] Mihara, T., Nakajima, M., Sugizaki, M., Serino, M., Matsuoka, M., Kohama, M., Kawasaki, K., Tomida, H., Ueno, S., Kawai, N., Kataoka, J., Morii, M., Yoshida, A., Yamaoka, K., Nakahira, S., Negoro, H., Isobe, N., Yamauchi, M., and Sakurai, I., "Gas Slit Camera (GSC) onboard MAXI on ISS," *Publ. Astron. Soc. Japan* **63**, S623–S634 (2011).

[21] Nakajima, H., Maeda, Y., Uchida, H., Tanaka, T., Tsunemi, H., Hayashida, K., Tsuru, T. G., Dotani, T., Nagino, R., Inoue, S., Ozaki, M., Tomida, H., Natsukari, C., Ueda, S., Mori, K., Yamauchi, M., Hatsukade, I., Nishioka, Y., Sakata, M., Beppu, T., Honda, D., Nobukawa, M., Hiraga, J. S., Kohmura, T., Murakami, H., Nobukawa, K. K., Bamba, A., Doty, J. P., Iizuka, R., Sato, T., Kurashima, S., Nakaniwa, N., Asai, R., Ishida, M., Mori, H., Soong, Y., Okajima, T., Serlemitsos, P., Tawara, Y., Mitsuishi, I., Ishibashi, K., Tamura, K., Hayashi, T., Furuzawa, A., Sugita, S., Miyazawa, T., Awaki, H., Miller, E. D., and Yamaguchi, H., "In-orbit performance of the soft X-ray imaging system aboard Hitomi (ASTRO-H)," *Publ. Astron. Soc. Japan* **70**, 21 (2018).

[22] Bon, E., Jovanović, P., Marziani, P., Shapovalova, A. I., Bon, N., Borka Jovanović, V., Borka, D., Sulentic, J., and Popović, L. Č., "The First Spectroscopically Resolved Sub-parsec Orbit of a Supermassive Binary ck Hole," *Astrophys. J.* **759**, 118 (2012).

[23] Snowden, S. L., McCammon, D., Burrows, D. N., and Mendenhall, J. A., "Analysis procedures for ROSAT XRT/PSPC observations of extended objects and the diffuse background," *Astrophys. J.* **424**, 714–728 (1994).

[24] Fujimoto, R., Mitsuda, K., Mccammon, D., Takei, Y., Bauer, M., Ishisaki, Y., Porter, S. F., Yamaguchi, H., Hayashida, K., and Yamasaki, N. Y., "Evidence for Solar-Wind Charge-Exchange X-Ray Emission from the Earth's Magnetosheath," *Publ. Astron. Soc. Japan* **59**, 133–140 (2008).

[25] Carter, J. A. and Sembay, S., "Identifying XMM-Newton observations affected by solar wind charge exchange. Part I," *A&A* **489**, 837–848 (2008).

[26] Ezoe, Y., Ebisawa, K., Yamasaki, N. Y., Mitsuda, K., Yoshitake, H., Terada, N., Miyoshi, Y., and Fujimoto, R., "Time Variability of the Geocoronal Solar-Wind Charge Exchange in the Direction of the Celestial Equator," *Publ. Astron. Soc. Japan* **62**, 981–986 (2010).

[27] Ezoe, Y., Miyoshi, Y., Yoshitake, H., Mitsuda, K., Terada, N., Oishi, S., and Ohashi, T., "Enhancement of Terrestrial Diffuse X-Ray Emission Associated with Coronal Mass Ejection and Geomagnetic Storm," *Publ. Astron. Soc. Japan* **63**, S691–S704 (2011).

[28] Ishikawa, K., Ezoe, Y., Miyoshi, Y., Terada, N., Mitsuda, K., and Ohashi, T., "Suzaku Observation of Strong Solar-Wind Charge-Exchange Emission from the Terrestrial Exosphere during a Geomagnetic Storm," *Publ. Astron. Soc. Japan* **65**, 63 (2013).

[29] Funase, R. and Team, E. P., "EQUULEUS: A 6U CubeSat to Fly to Earth—Moon Lagrange Point onboard SLS EM-1," in [*LCPM-12*], (2017).

[30] Robertson, I. P., Collier, M. R., Cravens, T. E., and Fok, M.-C., "X-ray emission from the terrestrial magnetosheath including the cusps," *J. Geophys. Res.* **111**, A12105 (2006).

[31] Treis, J., Andricek, L., Aschauer, F., Heinzinger, K., Herrmann, S., Hilchenbach, M., Lauf, T., Lechner, P., Lutz, G., Majewski, P., Porro, M., Richter, R. H., Schaller, G., Schnecke, M., Schopper, F., Soltau, H., Stefanescu, A., Strüder, L., and de Vita, G., "MIXS on BepiColombo and its DEPFET based focal plane instrumentation," *Nucl. Inst. Methods A* **624**, 540–547 (2010).

[32] Yoshino, T., Mitsuda, K., Yamasaki, N. Y., Takei, Y., Hagihara, T., Masui, K., Bauer, M., McCammon, D., Fujimoto, R., Wang, Q. D., and Yao, Y., "Energy Spectra of the Soft X-Ray Diffuse Emission in Fourteen Fields Observed with Suzaku," *Publ. Astron. Soc. Japan* **61**, 805–823 (2009).

[33] Kasahara, S., Ezoe, Y., Kimura, T., and Miyoshi, Y., "Radiation background and dose estimates for future X-ray observations in the Jovian magnetosphere," *Planet. Space Sci.* **75**, 129–135 (2013).

[34] The SMILE mission : http://sci.esa.int/smile/.

[35] The CuPID mission : http://sites.bu.edu/cupid/.

[36] Takeuchi, K., Ezoe, Y., Ishikawa, K., Numazawa, M., Terada, M., Ishi, D., Fujitani, M., Sowa, M., T., O., and K., M., "Pt thermal atomic layer deposition for silicon x-ray micropore optics," *Appl. Opt.* **57**, 3237–3243 (2018).

[37] Ogawa, T., Ezoe, Y., Moriyama, T., Mitsuishi, I., Kakiuchi, T., T., O., K., M., and Putkonen, M., "Iridium-coated micropore x-ray optics using dry etching of a silicon wafer and atomic layer deposition," *Appl. Opt.* **52**, 5949–5956 (2013).

[38] The ROSAT all sky survey : http://www.xray.mpe.mpg.de/cgi-bin/rosat/rosat-survey.